MATTER: International Journal of Science and Technology
ISSN 2454-5880

Pfennig & Kranzmann, 2019

Volume 5 Issue 1, pp. 138-158

Date of Publication: 19th April, 2019

DOI-https://dx.doi.org/10.20319/mijst.2019.51.138158

This paper can be cited as: Pfennig, A., & Kranzmann, A. (2019). Corrosion and Fatigue of Heat Treated Martensitic Stainless Steel 1.4542 used for Geothermal Applications. MATTER: International Journal of Science and Technology, 5(1), 138-158.

CORROSION AND FATIGUE OF HEAT TREATED MARTENSITIC STAINLESS STEEL 1.4542 USED FOR GEOTHERMAL APPLICATIONS

Anja Pfennig
HTW-Berlin, University of Applied Sciences, Berlin, Germany
anja.pfennig@htw-berlin.de

Axel Kranzmann
BAM, Federal Institute for Materials Research and Testing Berlin, Berlin, Germany
axel.kranzmann@bam.de

Abstract

During capture and storage technology (CCS) as well as in geothermal energy production steels need to withstand the corrosive environment such as: heat, pressure, salinity of the aquifer and CO_2-partial pressure. 1.4542 shows unusual corrosion phenomena, but is still sufficiently resistant in corrosive environments. To better understand its behaviour differently heat treated coupons of 1.4542 and for comparison X20Cr13 and X46Cr13 were kept in the artificial brine of the Northern German Basin at T=60 °C. Ambient pressure as well as p=100 bar for 700 h - 8000 h in water saturated supercritical CO_2 and CO_2-saturated synthetic aquifer environment was applied. Fatigue tests were performed via push-pull tests with a series of 30 specimens from 150 MPa to 500 MPa (sinusoidal dynamic test loads, R=-1; resonant frequency ~ 30 Hz). $FeCO_3$ and FeOOH are corrosion products also after dynamic corrosion tests. Martensitic microstructure offers good corrosion resistance in geothermal environment. The S-N-curve showing no typical fatigue strength and very steep slopes of possible fatigue strength for finite life. Possible influencing artefacts, such as Al-inclusions could not be correlated to early rupture

despite specimens containing inclusions at the fracture surface and cross section reached lower number of cycles. Applied potential proofed to enhance fatigue life tremendously.

Keywords

High Alloyed Steel, Pitting; Corrosion Fatigue, Corrosion, Endurance Limit, CCS, CO_2-Storage

1. Introduction

Emission gasses e.g. from combustion processes of power plants are compressed into deep geological saline aquifers CCS-site (CCS Carbon Capture and Storage (Thomas, 2005; van den Broek, Hoefnagels, Rubin, Turkenburg, Faaij, 2010)) will result in corrosion of piping and casing of the CCS engineering site (Nešić, 2007; Hurter, 2008; Zhang, Yang, Sun, Lu, 2008; Mu and Zhao, 2009; Seiersten, 2001; Cui, Wu, Uhu, Yang, 2006; Pfennig and Kranzmann, 2011). Injection pipe steels are highly sensitive towards CO_2-corrosion regarding alloy composition, contamination of alloy and media, temperature, CO_2 partial pressure, flow conditions and protective passivating corrosion scales (Zhang, Yang, Sun, Lu, 2008; Mu and Zhao, 2009; Zhang, Zhao, Juang, 2005; Alhajji and Reda, 1993; Choi and Nešić, 2008; Jiang, Nešić, Huet, 2008; Ahmand, Allam, Abdul Aleem, 2000; Pfennig and Bäßler, 2009; Pfennig and Kranzmann, 2010; Pfennig, Zastrow, Kranzmann, 2013; Nybor, 2005; Carvalho, Joia, Mattos, 2005; Linter and Burstein, 1999; Wu, Cui, Zhao, Yan, Zhu, Yang, 2004).

Alloying elements (Bülbül and Sun, 2010) and heat treatment (duration, temperature of initial austenitizing and annealing as well as cooling rate (Hou, Li, Li, Zhang, 2000; Cijović and Radenković, 2006; Park and Park, 2007)) significantly influence the corrosion behaviour of steels. In general Ni- and Cr contents (Banaś, Lelek-Borkowska, Mazurkiewicz, Solarski, 2007; Bilmes, Llorente, Méndez, Gervasi, 2009) improve the corrosion resistance. Retained austenite improves pitting corrosion resistance (Banaś et al., 2007). Higher austenitizing temperature for martensitic steels (Zhang et al., 2001; Brown, Parakala, Nešić 2004; Isfahany, Saghafian, Borhani, 2011) and annealing at higher temperature of lean duplex stainless steels (Bulbül and Sun, 2010; Hou et al., 2000; Zhang et al., 2001) decrease the susceptibility towards local corrosion. NaCl solution containing H_2S severely degrades Mn-containing carbon steels with martensitic microstructure compared to ferritic or ferritic-bainitic microstructures (Lucio-Garciaa et al., 2009) due to reactive grain boundaries in martensitic microstructures.

Locally corroded samples -with pits acting as corrosion catalyzer- usually reveal similar corrosion products as the slowly growing surface layers (Pfennig and Bäßler, 2009; Pfennig et

al., 2013). Generally siderite $FeCO_3$ (Nešić, 2007; Han, Yang, Nešić, 2008; Pfennig, Wolthusen, Zastrow, Kranzmann, 2015) precipitates on steels in contact with CO_2-environment because the solubility of $FeCO_3$ in water is low (p_{Ksp} = 10.54 at 25 °C (Brown et al., 2004; Han et al. 2008)) and consequently anodic iron dissolution takes plase. Transient $Fe(OH)_2$ is formed initially (Mu and Zhao, 2009; Isfahany et al., 2011) which may locally increase the pH in proximity to the hydroxide film followed by the consecutive formation an internal and external ferrous carbonate (Han et al., 2008) according to equations 1 to 6 (Pfennig and Bäßler, 2011; Brown et al., 2004):

$$CO_2\,(g) + H_2O\,(l) \rightarrow H^+ + HCO_3^-(aq) \quad (1)$$

cathodic: $$2\,HCO_3^- + 2\,e^- \rightarrow 2\,CO_3^{2-} + H_2 \quad (2)$$

anodic: $$Fe \rightarrow Fe^{2+} + 2e^- \quad (3)$$

$$Fe^{2+} + CO_3^{2-} \rightarrow FeCO_3 \quad (4)$$

$$Fe^{2+} + 2\,HCO_3^- \rightarrow Fe(HCO_3)_2 \quad (5)$$

$$Fe(HCO_3)_2 \rightarrow FeCO_3 + CO_2 + H_2O \quad (6)$$

Corrosion layers and pitting have been reported to cause early failure of materials under cyclic load (Madduri and Prakash, 2010; Msahiro, 1999; Vignal, Delrue Peultier, Oltra, 2007). Local corrosion on stainless steels is enhanced by

- Chemical corrosion reactions,
- Changes of lattice energy locally within the steel`s surface and
- Mechanical load (Pfennig, Wolf, Böllinghaus, 2016; Pfennig, Wiegand, Wolf, Bork, 2013).

Cracks are initiated and crack propagation is enhanced and accelerated at dual or triple points of grain/phase boundaries where the grain/phase boundary energy is higher (Madduri and Prakash, 2010; Vignal et al., 2007). The local lattice mismatch at grain/phase boundaries also initiates pit formation, selective corrosion and inter granular deterioration resulting crack formation (Masahiro, 1999).

Parts of this work have been presented at GHGT13 (Pfennig et al., 2015), ICFEE 2017 (Pfennig and Kranzmann, 2017) and ICBEE 2019 (to be published) and we will now give an update on new findings, summarize all our previous work of the last 10 year and compare results to heat treated martensitic stainless steels (1.4022 and 1.4043). This is our final review work on corrosion kinetics of X20Cr13, X46Cr13 and X5CrNiCuNb16-4. Further investigation will comprise the corrosion mechanism, respectively.

2. Materials and Methods

Both, immersion tests as well as corrosion fatigue tests were undertaken for the same steel quality (martensitic AISI 630, X5CrNiCuNb16-4, 1.4542, tensile strength in air: 1078 MPa) (Table 1)) using synthesized Stuttgart Aquifer (Förster et al., 2006): Ca^{2+}: 1760 mg/L, K^{2+}: 430 mg/L, Mg^{2+}: 1270 mg/L, Na^{2+}: 90,100 mg/L, Cl^{-}: 143,300 mg/L, SO_4^{2-}: 3600 mg/L, HCO_3^{-}: 40 mg/L). For fatigue tests the surfaces were activated via machining to Rz=4.

Table 1: *Element distribution of 1.4542 (X5CrNiCuNb16-4, AISI 630), (mass percent)*

Element	C	Si	Mn	P	S	Cr	Mo	Ni	Cu	Nb
acc standard [a]	≤ 0.07	≤ 0.70	≤ 1.50	≤ 0.04	≤ 0.015	15.0 - 17.0	≤ 0.60	3.00 – 5.00	3.00 – 5.00	0.20 – 0.45
analysed [b]	0.03	0.42	0.68	0.018	0.002	15.75	0.11	4.54	3.00	0.242

a) elements in accordance to **DIN EN 10088-3 in %**
b) measured via spark emission spectrometry

Heat treatment (Table 2), sample preparation, laboratory scale exposure tests using coupons (8 mm thickness, 20 mm width, 50 mm length) and corrosion fatigue tests as well as electrochemical in-situ and optical analysis procedures have been widely described in detail in our previous work (Pfennig and Bäßler, 2009; Wolf, Afanasiev, Böllinghaus, Pfennig, 2016; Pfennig and Kranzmann, 2017, Pfennig, Heynert, Wolf, Böllinghaus, 2014)

Table 2: *Heat Treatment Protocol for X5CrNiCuNb16-4*

Heat Treatment	**Temperature**	**Time**	**Cooling Medium**
	°C / °C	**in min**	
normalizing	850	30	oil
hardening	1040	30	oil
hardening and tempering 1, 550 °C	1040 / 550	30	oil
hardening and tempering 2, 650 °C	1040 / 650	30	oil
hardening and tempering 3, 755 °C	1040 / 755	30	oil

Temperature, pH and electrochemical potential were measured directly within the corrosion chamber using an Ag/AgCl wire electrode fixed in a Teflon channel to measure the open-circuit electrochemical potential. Fatigue tests were carried out at 30 – 40 Hz in stress-strain mode under CCS aquifer environment with additional technical CO_2 (flow rate. 9 L/h). Temperature fluctuation was kept below ± 0.3 K and mean frequency of the cyclic load accounted to 30-33 Hz.

3. Results and Discussion

According to DIN 6601 the following equation was used to calculate surface corrosion rates:

$$\text{Corrosion rate: } \omega = \frac{8760\left[\frac{mm}{year}\right] * 10\left[\frac{mm}{cm}\right] * weight\ loss[g]}{area[cm^2] * density\left[\frac{g}{cm^3}\right] * time[hour]} \quad (7)$$

Corrosion rates obtained after exposure to the liquid phase are much higher (by a factor of 3 after 8000 h of exposure) indicating the different reaction kinetics in different atmospheres. Diffusion in the liquid phase is slower prohibiting the precipitation of a continuous passivating corrosion layer whereas fast diffusion allows for the formation of a protective corrosion layer rather quickly.

3.1 Surface Corrosion

Samples exposed to the vapour phase (water saturated CO_2) show no dependence on exposure time or method of heat treatment. Corrosion rates remain nearly constant at approximately 0.004 mm/year. The carbonate layer is sufficient thick and can act as a diffusion barrier and reducing mutual diffusion of ions (CO_3^{2-}- and O^{2-}-species) into the steel and Fe-ions towards the outer surface (Pfennig et al., 2015).

In the liquid phase (CO_2-saturated saline aquifer) the corrosion rates increase, then decrease due to the formation of a passivating layer, and then increase again. This phenomenon (increase/decrease) is stronger for coupons immersed into the CO_2-saturated brine (corrosion rates around 0.004 to 0.014 mm/year). This may be due to the break-down of the passivating layer allowing the rather fast mutual diffusion of gaseous CO_3^{2-}- and O_2 -species into the metal and iron towards the surface where mainly siderite $FeCO_3$ layers are formed (Figure 1) (Pfennig et al, 2013; Pfennig, Wiegand et al., 2013). Large areas of the corrosion layer may locally detach lateral to the surface enhancing and accelerating new processes at a fresh surface. Specimens exposed to CO_2-saturated saline aquifer form a carbonate layer because the siderite $FeCO_3$-solubility in CO_2-containing water with rather low pH is low after carbonic acid has formed (Cvijović and Randković, 2006). These heterogeneous corrosion scales of different magnitude cover the specimens` surface and pits. Main phases are: siderite $FeCO_3$ and cementite Fe_3C. Also, goethite α-FeOOH at 100 bar and mackinawite FeS, akaganeite $Fe_8O_8(OH)_8Cl_{1.34}$ and spinel-phases of various compositions are present at ambient pressure (Pfennig et al., 2015; Pfennig and Kranzmann, 2017).

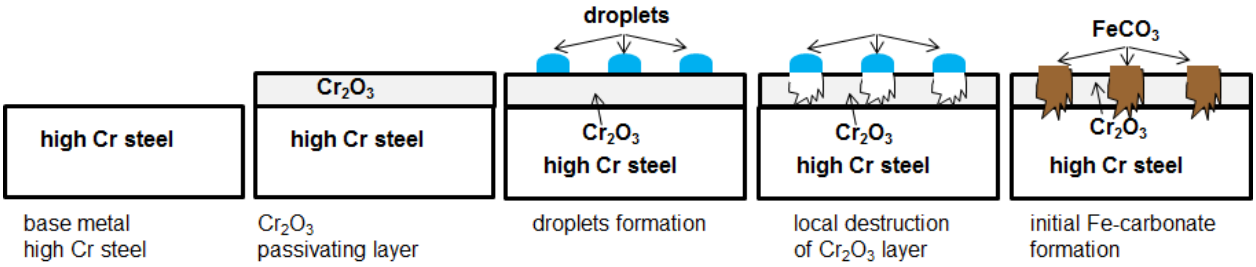

Figure 1: *Schematic drawing of the precipitation of the corrosion layer on 1.4542 and example of sample surfaces after 8000 h of exposure to water saturated supercritical CO_2*

Han et al., 2008 introduced a crack initiation model which was modified by Pfennig et al., 2016, 2013) applying for all states of heat treatment after exposure to CCS environment at 60 °C.

The three phase boundary during intermission of the CCS-process leads an unusual corrosion formation characterized by corroded ellipsoidal regions (Pfennig et al., 2017; Pfennig et al., 2016; Pfennig, Wolthusen, Wolf, Kranzmann, 2014). Siderite $FeCO_3$ and goethite α-FeOOH passivate the remaining surfaces. The leopard structure is a consequence of the decreasing water solubility in supercritical carbon dioxide (Banaś et al., 2007). As shown in Figure 1 thin and small water droplets cover the metal surface that then consolidate (Pfennig et al., 2016). The initial ferrous hydroxide film is mechanically and/or chemically damaged and the highly porous non-protective ferrous carbonate is exposed directly to the geothermal water. Because these reactions result in a decreasing pH of the surrounding water the ferrous carbonate film dissolves and the steel depassivates. Then small pits that contain sulphates ($FeSO_4$) precipitating from the brine are formed and centered on the edges of former droplets (Figure 1). The former droplet center mainly reveals hematite (Fe_2O_3) (Han et al., 2008; Pfennig and Kranzmann, 2017). The flowing corrosive media removes the remaining film causing the pit to grow wider.

Independent of heat treatment, atmosphere (liquid, supercritical/vapour) or pressure (1 bar, 100 bar) the corrosion rate for X20Cr13 and X46Cr13 as well as X5CrNiCuNb16-4 is below 0.04 mm/year. High pressure in accordance with high CO_2 partial pressure reduced corrosion reactions and the lower corrosion rates after long exposure are likely to blocked capillaries within corrosion layers of adequate thickness that prevent fast diffusion. Therefore supercritical CO_2 possesses inhibiting function.

The influence of the corrosion behavior on the heat treatment of steels prior to exposure has been widely described (Alhajii and Reda, 1993; Pfennig et al., 2013; Bülbül and Sun, 2010; Zhang et al., 2008; Bron et al, 2004; Pfennig et al., 2014; Pfennig et al., 2017) (Figure 2). All corrosion rates of the steels investigated in this study increase with exposure time. Whereas in comparison to X5CrNiCuNb16-4 the corrosion rates of both heat treated martensitic steels X20Cr13 and X46Cr13 strongly increase by a factor of 3 at ambient pressure there is no increase at 100 bar (Figure 2) from 4000 h to 8000 h.

With exception of steel specimen hardened and tempered at 700 °C the corrosion rates of X20Cr13 and X46Cr13 are similar at 100 bar to those measured for the higher alloyed steel X5CrNiCuNb16-4 (below 0.005 mm/year). After long exposure times all specimen show similar corrosion rates with exception of steel specimen of X20Cr13/X46Cr13 hardened and tempered at 700/755 °C. Possibly chromium carbides precipitate and deplete the metal matrix so that no chromium oxide passivation layer may be formed and the steel degrades after long exposure times.

At 100 bar all graphs are parallel indicating that the heat treatment seems to influence the corrosion rate less than at ambient pressure. It may be assumed that heat treatment for X5CrNiCuNb16-4 plays a minor role with chromium content and atmosphere being more decisive. Hardened or hardened and tempered coupons give lowest corrosion rates at ambient pressure (Figure 2). Taking into account surface corrosion only, at 100 bar martensitic microstructure (hardened and tempered at 650 °C for the supercritical phase: < 0.001 mm/year) is preferred in water saturated supercritical CO_2. In CO_2 saturated aquifer water, however, normalized microstructure show good corrosion resistance (ca. 0.004 mm/year) (Pfennig et al., 2016).

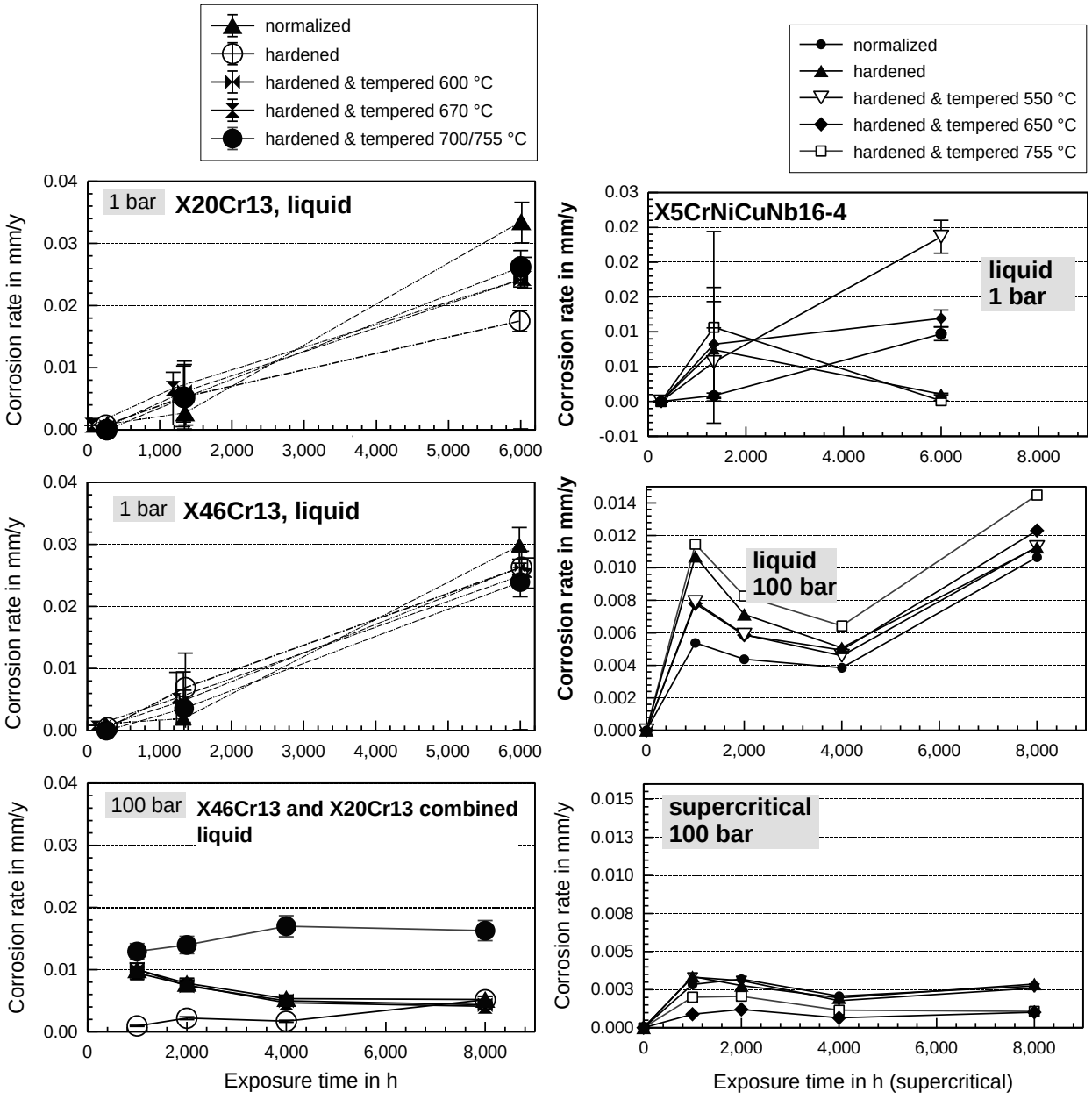

Figure 2: *The role of heat treatment on the corrosion rate of X5CrNiCuNb16-4 at 60 °C exposed to CO_2 saturated saline aquifer water at 1 bar and 100 bar (top (Pfennig et al., 2013; Pfennig and Kranzmann 2014) and in water saturated supercritical CO_2 (bottom) at 100 bar (Pfennig et al., 2013) in comparison to the corrosion rate of X20Cr13 and X46Cr13 (Pfennig et al., 2013; Pfennig et al., 2014).*

In general corrosion rates for X5CrNiCuNb16-4 are low due to the passivating nature of the steel with even lower corrosion rates in the supercritical than in the liquid phase. Possible explanations are the lack of electrolytes (Pfennig et al., 2013; Pfennig et al., 2016) or the cathodic reactions described in equation (1) and (2). With a higher H_2CO_3 concentration the

environment becomes more acidic and reactive compared to the CO_2 saturated liquid phase (Seiersten, 2001; Banaś et al., 2007). For X5CrNiCuNb16-4 all corrosion rates increase at 100 bar in the supercritical phase indicating fast reaction kinetics and depassivation of the steel surface while the corrosion rates for specimen kept in the aquiver water remain at approximately 0.003 mm/y after 4000h and do not increase further with no regard to heat treatment. Due to carbide formation the initial passivating layer deteriorates after 1000 h of exposure (Figure 3, left). Because chromium is used to form carbides surface passivation –dependent on excess free chromium- is prohibited (Pfennig et al., 2016).

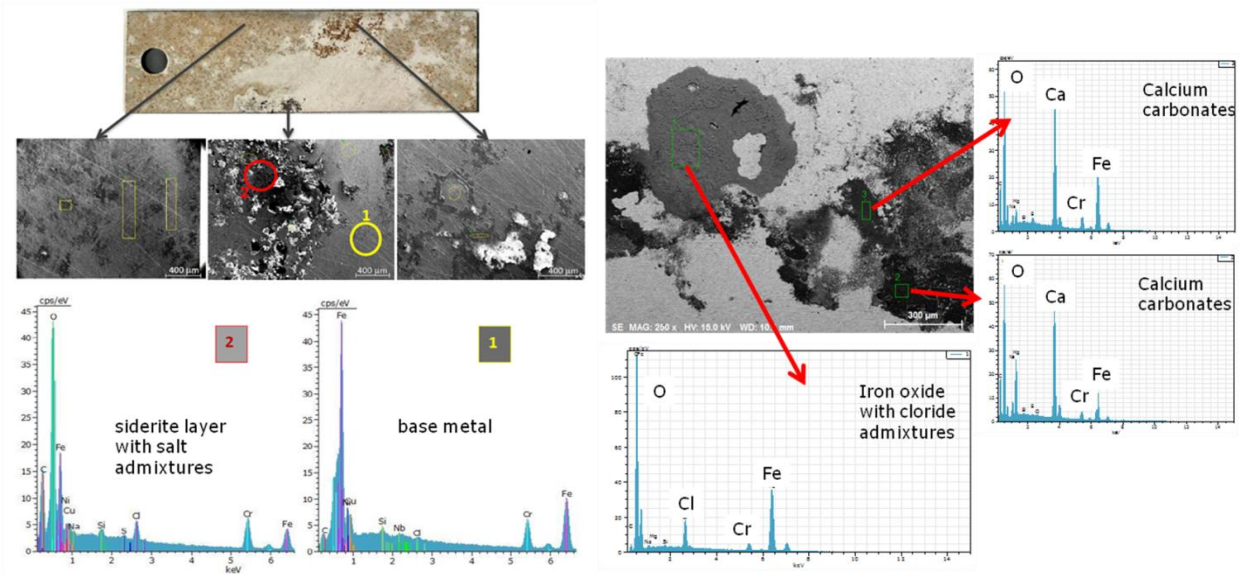

Figure 3: left: *SEM micrographs and composition of the ellipsoidal corrosion layer formed on 1.4542 hardened and tempered at 670 °C prior to exposure after 8000 hours of exposure at 60 °C and 100 bar to water saturated supercritical CO_2;*

3.2 Local Corrosion

Pit intrusion depths generally increase with exposure time (Figure 4). Because pits reveal similar corrosion products as the surface corrosion layer it is necessary to separate these from saline precipitations such as $CaCO_3$ as seen in Figure 3, right. The presence of chlorides enhances local corrosion of the microstructure (Pfennig et al., 2016) as well as a high number of dislocations, grain boundaries, precipitation at phase boundaries, such as carbides. As a consequence local lattice mismatch leads to higher local boundary energy (Vignal et al., 2007) leaving the steel highly susceptible to corrosive attack of the CCS environment.

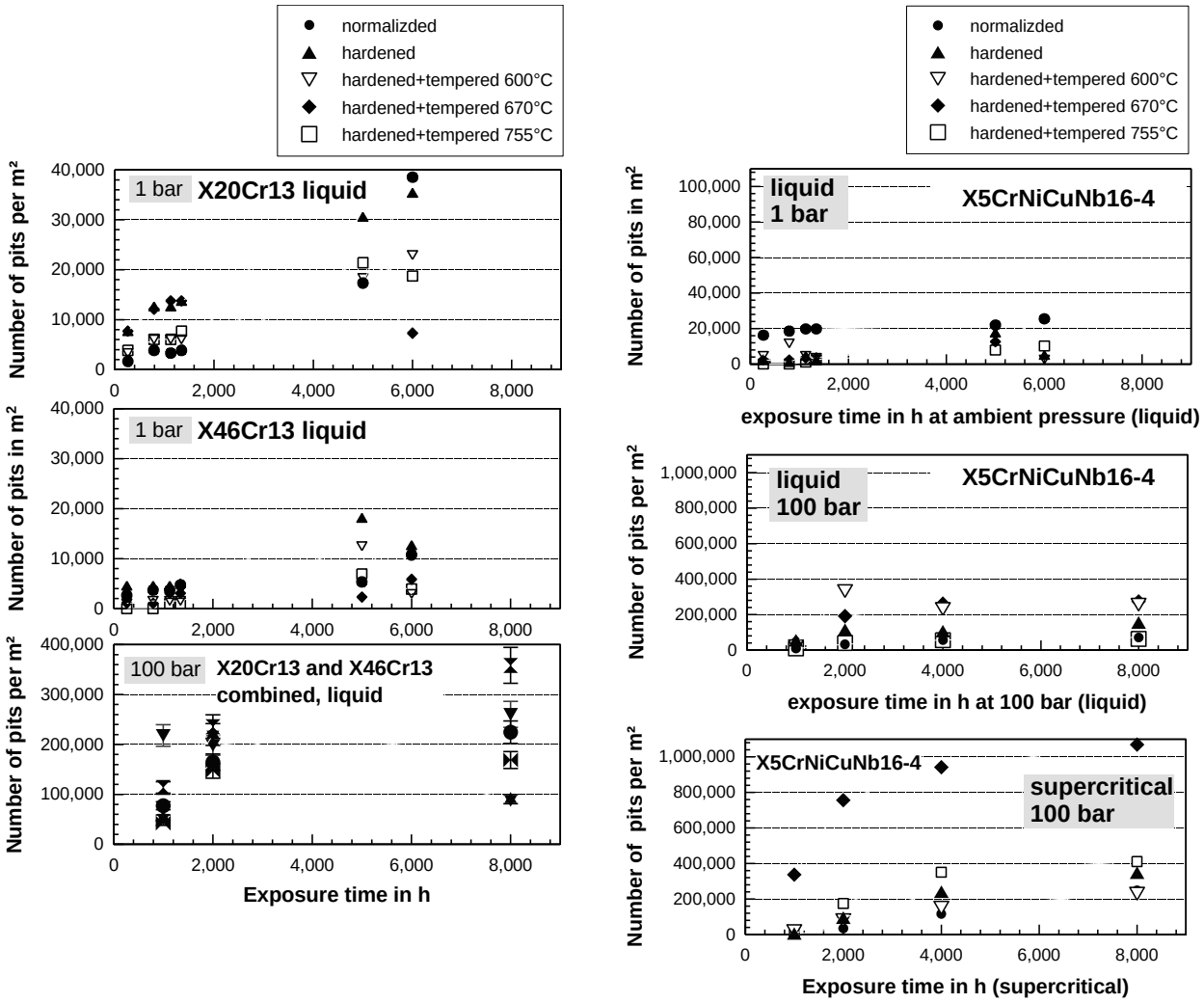

Figure 4: *The role of heat treatment on the local corrosion of X5CrNiCuNb16-4 at 60 °C exposed to CO_2 saturated saline aquifer water at 1 bar and 100 bar (top partly taken from Pfennig et al., 2016 and in water saturated supercritical CO_2 (bottom) at 100 bar (Pfennig et al., 2013).Results are compared to the local corrosion of X20Cr13 at 60 °C, partly taken from Pfennig et al., 2013 and Pfennig et al., 2014*

Overall the penetration depth is independent of the heat treatment, showing lower intrusion depth (8-25 µm) for X20Cr13 and X46Cr13 after normalizing and hardening+tempering at 600 °C (Maximum intrusion depths ca. 300 µm for hardened X20Cr13 and a little lower for X46Cr13). For X5CrNiCuNb16-4 hardening+tempering from 670 °C to 755 °C offer low penetrations depths (10µm) (Pfennig et al., 2014) (10-250 µm average pit depths after exposure at 100 bar and 60 °C).

Figure 4 (Pfennig et al., 2013; Pfennig et al., 2016) normalizes comparable results obtained for X20Cr13 and X46Cr13 revealing smallest number of pits after 6000 h for hardening

and tempering 600°C-670°C. Unusual low numbers of pits are likely because pits consolidate to shallow pits. At ambient pressure the number of pits are similar (<40,000 per m^2) for X20Cr13, X46Cr13 and X5CrNiCuNb16-4. At 100 bar X5CrNiCuNb16-4 shows a high number of pits per m^2 in both atmospheres (Figure 6) (Pfennig et al, 2014). In general the number of pits formed in the supercritical and liquid phase is the same with exception for samples heat treated and hardened and tempered at 670 °C. There is no significant dependence of local corrosion phenomena on the heat treatment prior to exposure. Although X5CrNiCuNb16-4 is known as corrosion resistant in CCS environment it exhibits a significantly high number of pits at ambient pressure and 100 bar.

3.3 Corrosion Fatigue

The distinct corrosion fatigue behavior was described earlier by Pfennig et al. 2017, Pfennig et al., 2016 and Wolf et al., 2016). But, because these results were very unusual the fatigue tests were redone with a different charge of samples and newly artificially produced laboratory aquifer water (Figure 5). These results have been presented at ICBEE 2018.

Earlier results showed that the S-N-curve did not show expected fatigue strength and non-linear very steep slopes of possible fatigue strength for finite life (Wöhler-exponent of k = 3.59, scatter range TN=1:34, very small coefficient of correlation r^2 = 0.33), max. number of cycles (10 x 10^7) at S_a=150 MPa) (Figure 6, bottom). Although the scatter range is much smaller, the slope of the fatigue limit line is still very steep indicating fast degradation of the material and resulting in an even lower max. number of cycles (10x10^7) at S_a=130 MPa). The corrosion fatigue strength of X5CrNiCuNb16-4 is 60% lower than the endurance limit measured in air (620 MPa) (Pfennig et al., 2016), with steeper slope of the fatigue limit line as a function of increasing number of cycles (Pfennig and Kranzmann, 2017; Wolf et al., 2016).

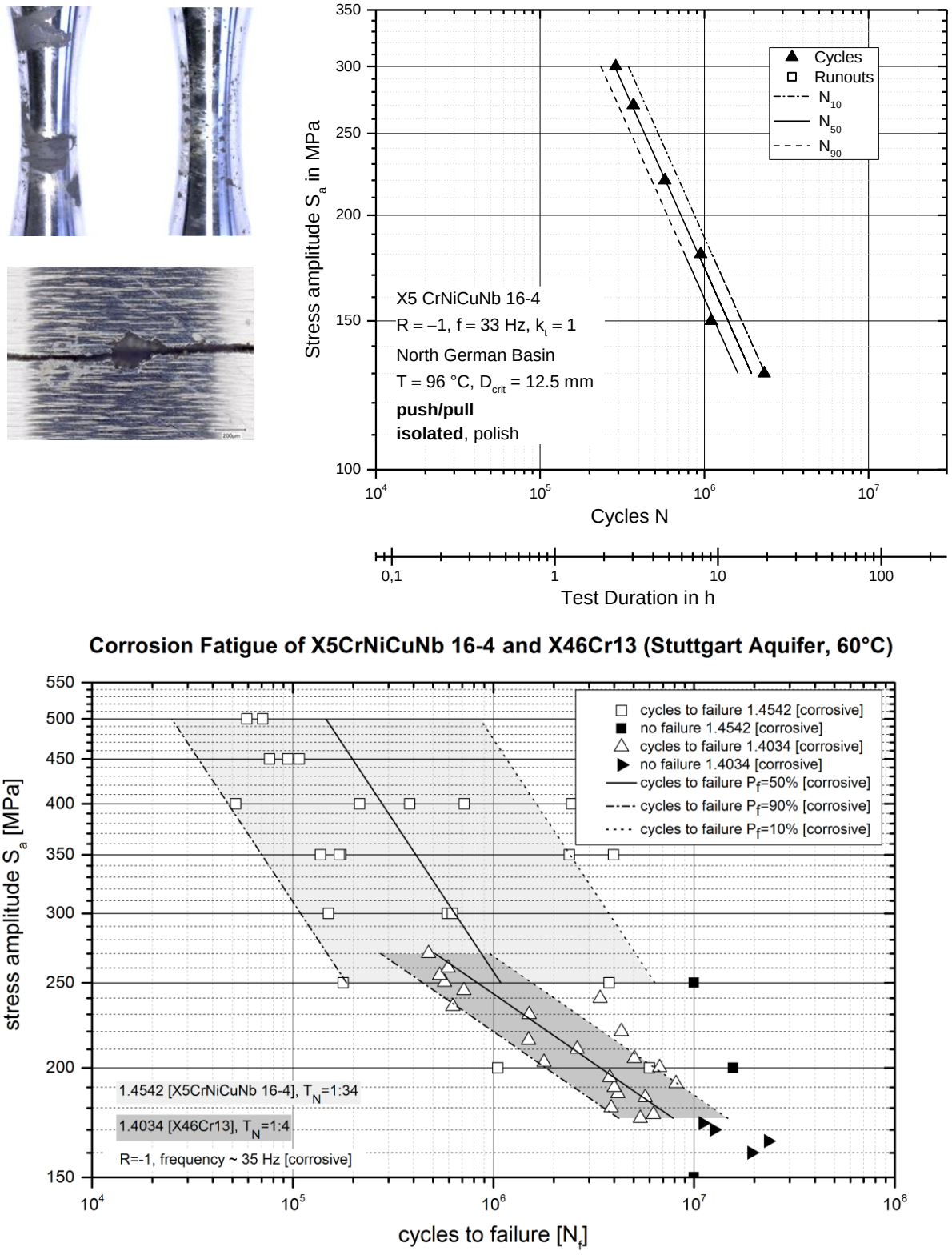

Figure 5: *S-N-curve and crack formation on 1.4542 exposed to saline aquifer water and technical CO_2. For comparison results from former experiments are given (Wolf et al., 2016)*

No correlation was found regarding artificial aquifer water (Pfennig and Kranzmann, 2017) stress amplitude and number of failures, with increasing stress not inevitably leading to a lower number of cycles as expected. However, Aluminium was measured and heterogeneously distributed non-metallic inclusions were detected in the martensitic structure embedded with δ-ferrite (Figure 6, bottom) for samples with presumably short number of cycles to failure (Pfennig et al., 2016). This finding is appointed to this particular charge of the alloy, because in general it could not clearly be stated that Aluminum found within the microstructure leads to lower number of cycles and unpredictable early failure (Pfennig et al., 2017). X5CrNiCuNb16-4 reveals multiple cracks that are easily backtracked to pits as source of crack initiation. Inclusions, Aluminum and corrosion layer do not significantly influence the endurance limit – neither during the first fatigue testing nor the second. In general, early failure could not be related to

- Stress Amplitude,
- Impurities within the Microstructure
- Precipitation and Thickness of the Corrosion Layer
- Number of Striations.

As a consequence of the mechanical load the local boundary energy within the microstructure of the steel is increased due to local lattice mismatch (Pfennig et al, 2013) resulting in enhanced local corrosion as a result of:

- chlorides (Unigovski et al., 2009)
- Increased Dislocation Number
- Grain Boundaries
- Precipitation Phase Boundaries and Carbides.

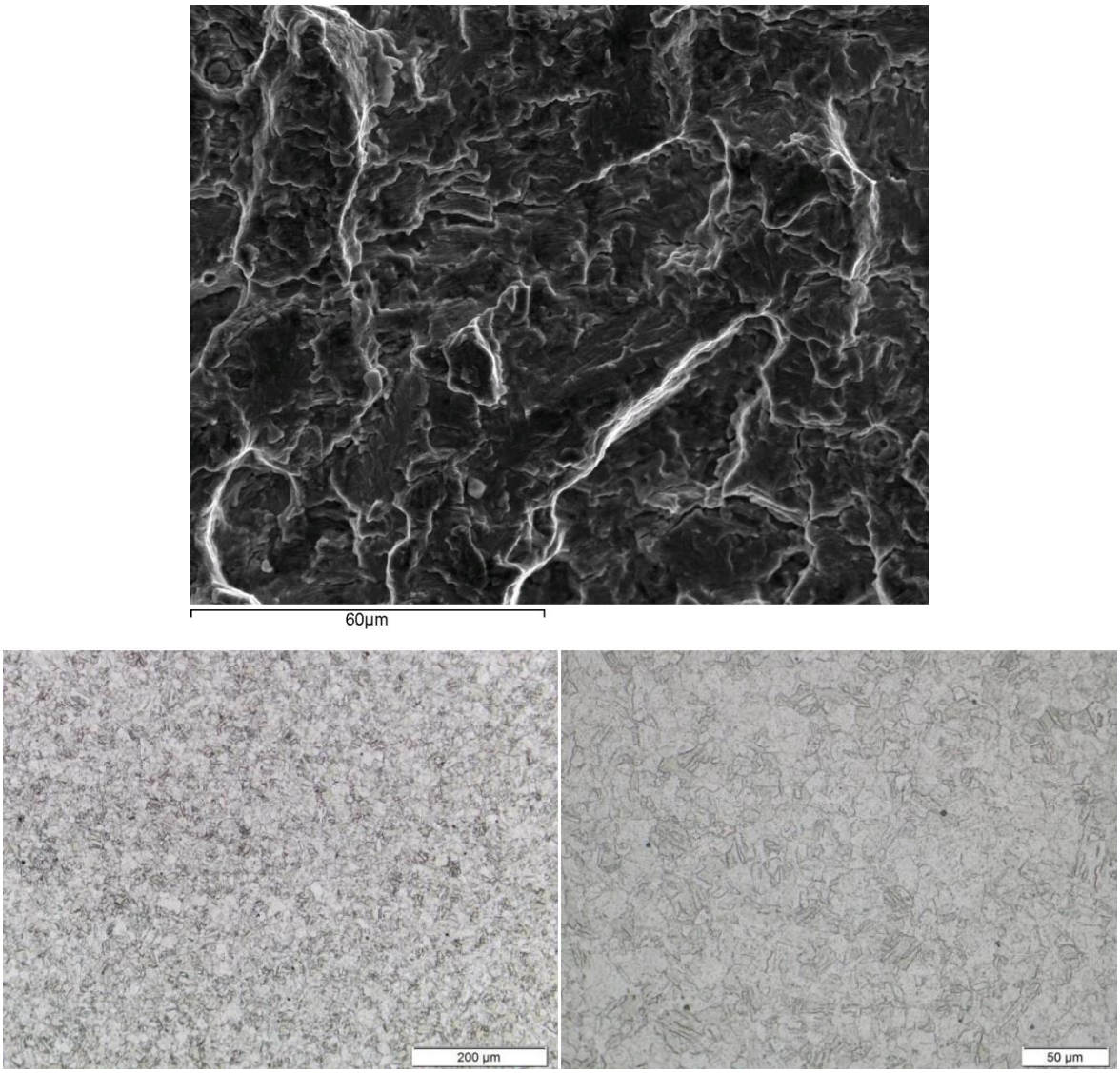

Figure 6: *Surface Image of Corrosion Layer on Fatigue Specimen Revealing Striations (Bottom) and Microstructure of X5CrNiCuNb16-4*

The application of a cathodic potential proofed to enhance the corrosion fatigue life expectancy by a factor of 20 to 70. The potentials U_{SHE} = –400 to –150 mV only covered cathodic domains (Figure 7). Depending on the potential applied the deterioration was slower (low potentials) or faster (high potentials). A decreasing potential leads to the increase of the alloy's corrosion fatigue life expectancy i.e. to an increase of number of cycles to failure. Runout specimens were loaded within the potentials U_{SHE} = –150 to –400 mV (preset threshold of 10^7 cycles, no mechanical failure). Note, a cathodic potential discharges hydrogen from the specimen's surface, enhances embrittlement of the alloy and may then lead to unpredicted and earlier failure.

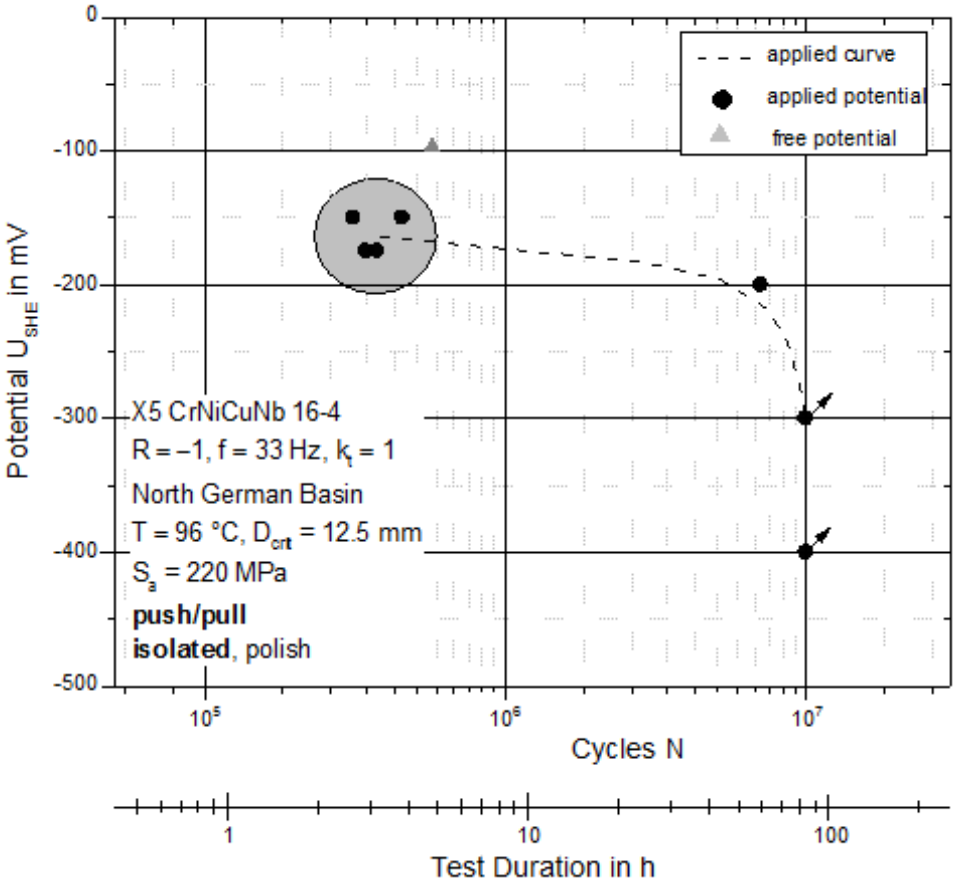

Figure 7: *CF life expectancy of X5CrNiCuNb16-4 with applied potential; isolated test set up, polished surface finish, push/pull load*

4. Conclusion

The corrosion process and corrosion fatigue behavior of martensitic stainless steel 1.4542 was investigated to predict reliability of the steel in geothermal environment. At 100 bar as well as at ambient pressure and 60 °C hardening and tempering at low temperatures (600 to 670 °C) for 1.4022, 1.4043 and 1.4542 result in lowest corrosion rates and reveal good resistance against local corrosion.

Surface corrosion resistance is better in supercritical CO_2, whereas pit corrosion resistance is better in CO_2 saturated brine. Non-uniform corrosion scales with differences in thickness cover the specimens` surface are mainly composed of: siderite $FeCO_3$ and carbides, mainly Fe_3C. Generally, ellipsoidal surface corrosion regions appear after exposure of >4000 h revealing hematite Fe_2O_3 and iron sulfate $FeSO_4$, $FeCO_3$ and FeOOH – the latter also after

corrosion fatigue tests. CCS environment cuts the endurance limit of 1.4542 measured in air in half. No significant correlation could be found between inclusions, discontinuous phase distribution, and Aluminum content within the base alloy and early rupture. Inclusions at the fracture surface and its cross section, pit and intercrystalline corrosion are source of crack formation lowering the number of cycles to failure.

Pitting corrosion phenomena, which most likely lead to a notch-based initiation region propagating fatigue crack growth, can be successfully depressed applying an appropriate cathodic potential. During geothermal application the fatigue life expectancy can therefore be enhanced to a great proportion by cathodic protection.

Acknowledgements

This work was supported by the FNK (Fachkonferenz für wissenschaftlichliche Nachwuchskräfte) of the Applied University of Berlin, HTW and by IMPACT (EU-Project EFRE 20072013 2/21). The authors would like to thank Andre Gröber, Rainer Wiegand, Roman Simkin and Roman Afanasiev for their worthy contribution to this paper.

References

Ahmad Z., Allam I.M., Abdul Aleem B.J. (2000). Effect of environmental factors on the atmospheric corrosion of mild steel in aggressive sea coastal environment, Anti Corrosion Methods and Materials, 47, 215-225 https://doi.org/10.1108/00035590010344312

Alhajji J.N. and M.R. Reda M.R. (1993). The effect of alloying elements on the electrochemical corrosion of low residual carbon steels instagnant CO_2-saturated brine, Corrosion Science, 34 (11) 1899-1911 https://doi.org/10.1016/0010-938X(93)90026-D

Banaś, J., Lelek-Borkowska, U., Mazurkiewicz B., Solarski W. (2007). Effect of CO2 and H2S on the composition and stability of passive film on iron alloy in geothermal water. Electrochimica Acta, 52, 5704–5714. https://doi.org/10.1016/j.electacta.2007.01.086

Bilmes P.D., Llorente C.L., Méndez C.M., Gervasi C.A. (2009). Microstructure, heat treatment and pitting corrosion of 13CrNiMo plate and weld metals, Corrosion Science, 51 (4), 876-882 https://doi.org/10.1016/j.corsci.2009.01.018

Brown B., Parakala S. R., Nešić S. (2004). CO_2 corrosion in the presence of trace amounts of H_2S, Corrosion, paper no. 04736, 1-28

Bülbül Ş., Sun Y. (2010). Corrosion behaviours of high Cr-Ni cast steels in the HCl solution. Journal of Alloys and Compounds, 598, 143-147 https://doi.org/10.1016/j.jallcom.2010.02.203

Carvalho D.S, Joia C.J.B, Mattos O.R. (2005). Corrosion rate of iron and iron-chromium alloys in CO_2-medium. Corrosion Science, 47, 2974-2986. https://doi.org/10.1016/j.corsci.2005.05.052

Choi, Y.-S. and Nešić, S. (2008). Corrosion behaviour of carbon steel in supercritical CO2-water environments. No. 09256 NACE Corrosion Conf. & Expo, New Orleans, Louisiana, USA, March 16th – 20th.

Cui, Z.D., Wu, S.L., Zhu, S.L., Yang, X.J. (2006). Study on corrosion properties of pipelines in simulated produced water saturated with supercritical CO_2. Applied Surface Science, 252, 2368-2374. https://doi.org/10.1016/j.apsusc.2005.04.008

Cvijović Z. and Radenković G. (2006). Microstructure and pitting corrosion resistance of annealed duplex stainless steel. Corrosion Science, 48,3887-3906 https://doi.org/10.1016/j.corsci.2006.04.003

Förster, A et al. (2010) Reservoir characterization of a CO2 storage aquifer: The Upper Triassic Stuttgart Formation in the Northeast German Basin. Mar. Pet. Geol., 27, 2156–2172 https://doi.org/10.1016/j.marpetgeo.2010.07.010

Förster, A., Norden, B. Zinck-Jørgensen, K. Frykman, P. Kulenkampff, J. Spangenberg, E. Erzinger, J. Zimmer, M. Kopp, J. Borm, G. Juhlin, C. Cosma, C. Hurter, S. (2006), Baseline characterization of the CO2SINK geological storage site at Ketzin, Germany: Environmental Geosciences, 13 (3), 145-161 https://doi.org/10.1306/eg.02080605016

Han J., Yang Y., Nešić S., Brown B. N (2008)., Roles of passivation and galvanic effects in localized CO_2 corrosion of mild steel, Paper No. 08332, NACE Corrosion 2008, New Orleans, Louisiana, USA, March 16th – 20th

Hou B., Li Y., Li Y., Zhang J. (2000). Effect of alloy elements on the anti-corrosion properties of low alloy steel, Bull. Mater. Sci, 23 (3), 189-192 https://doi.org/10.1023/A:1004722603945 https://doi.org/10.1023/A:1004832305979 https://doi.org/10.1023/A:1004718508280 https://doi.org/10.1023/A:1004755014553

Hurter S. (2008). Impact of Mutual Solubility of H_2O and CO_2 on Injection Operations for Geological Storage of CO_2, International Conference of the Properties of Water and Steem ICPWS, Berlin, September 8-11

Isfahany A. N., Saghafian H., Borhani G. (2011). The effect of heat treatment on mechanical properties and corrosion behaviour of AISI420 martensitic stainless steel, Journal of Alloys and Compounds, 509, 3931-3936 https://doi.org/10.1016/j.jallcom.2010.12.174

Jiang X., Nešić S., Huet F. (2008). The Effect of Electrode Size on Electrochemical Noise Measurements and the Role of Chloride on Localized CO_2 Corrosion of Mild Steel, Paper No. 09575, NACE Corrosion 2008 Conference and Expo, New Orleans, Louisiana, USA, March 16th – 20th

Kraus SW. and Nolze G. (1996). POWDER CELL – a program for the representation and manipulation of crystal structures and calculation of the resulting X-ray powder patterns, J. Appl. Cryst., 29, 301-303 https://doi.org/10.1107/S0021889895014920

Linter B.R., Burstein G.T. (1999). Reactions of pipeline steels in carbon dioxide solutions, Corrosion Science, 41,117-139 https://doi.org/10.1016/S0010-938X(98)00104-8

Lucio-Garciaa M.A., Gonzalez-Rodrigueza J.G., Casalesc M., Martinezc L., Chacon-Navaa J.G., Neri-Floresa M.A. and Martinez-Villafañea A. (2009). Effect of heat treatment on H_2S corrosion of a micro-alloyed C–Mn steel. Corrosion Science, 51, 2380-2386 https://doi.org/10.1016/j.corsci.2009.06.022

Madduri, C. and Prakash R. V. (2010). Corrosion Fatigue Crack Growth Studies in Ni-Cr-Mn steels, International Journal of Mechanical and Materials Engineerin,g 1, 20-25

Masahiro Seo, Electrochemical Society. Corrosion Division (2009). Passivity and localized corrosion: an International Symposium in Honour of Professor Norio Sato, initiation and stability of localized corrosion processes on stein steels. The Electrochemical Society, 483-490

Mu L.J., Zhao W.Z. (2010). Investigation on carbon dioxide corrosion behavior of HP13Cr110 stainless steel in simulated stratum water. Corrosion Science, 52, 82-89. https://doi.org/10.1016/j.corsci.2009.08.056

Nešić, S. (2007). Key issues related to modelling of internal corrosion of oil and gas pipelines – A review. Corrosion Science, 49, 4308–4338. https://doi.org/10.1016/j.corsci.2007.06.006

Nyborg R. (2005). Controlling Internal Corrosion in Oil and Gas Pipelines, Business Briefing: Exploration & Production: The Oil & Gas Review, 2, 70-74

Park J.-Y., Park Y.-S. (2007). The effects of heat-treatment parameters on corrosion resistance and phase transformation of 14Cr-3Mo martensitic stainless steel, Materials Science and Engineering A, 449-451, 1131-1134 https://doi.org/10.1016/j.msea.2006.03.134

Pfennig A., Bäßler R. (2009). Effect of CO_2 on the stability of steels with 1% and 13% Cr in saline water, Corrosion Science, 51 (4), 931-940 https://doi.org/10.1016/j.corsci.2009.01.025

Pfennig A., Heynert K., Wolf M., Böllinghaus T. (2014). First in-situ Electrochemical Measurement During Fatigue Testing of Injection Pipe Steels to Determine the Reliability of a Saline Aquifer Water CCS-site in the Northern German Basin. Energy Procedia, 63, 5773-5786. https://doi.org/10.1016/j.egypro.2014.11.610 https://doi.org/10.1016/j.egypro.2014.11.609

Pfennig A., Kranzmann A. (2010). The role of pit corrosion in engineering the carbon storage site Ketzin, Germany, WIT Transactions on Ecology and the Environment, 126, 109-118 https://doi.org/10.2495/AIR100101

Pfennig A., Kranzmann A. (2017). Potential of martensitic stainless steel X5CrNiCuNb 16-4 as pipe steel in corrosive CCS environment, International Conference on Future Environment and Energy ICFEE 2017, Penang, Malaysia, January 8th-10th 2017 https://doi.org/10.18178/ijesd.2017.8.7.998

Pfennig A., Wiegand R., Wolf M., Bork C.-P. (2013). Corrosion and corrosion fatigue of AISI 420C (X46Cr13) at 60 °C in CO2-saturated artificial geothermal brine, Corrosion Science, 68, 134–143 https://doi.org/10.1016/j.corsci.2012.11.005

Pfennig A., Wolf M., Böllinghaus Th. (2016). Corrosion Fatigue of X46Cr13 in CCS Environment, in Energy Technology 2016: Carbon Dioxide Management and Other Technologies, 1, 49-56

Pfennig A., Wolf M., Gröber A., Böllinghaus T., Kranzmann A. (2016). Corrosion fatigue of 1.4542 exposed to a laboratory saline aquifer water CCS-environment, 13th International Conference on Greenhouse Gas Control Technologies, GHGT-13, 14th -18th November 2016, Lausanne, Switzerland.

Pfennig A., Wolthusen H., Zastrow P., Kranzmann A. (2015). Evaluation of heat treatment

performance of potential pipe steels in CCS-environment, Carbon Dioxide Management and Other Technologies, 1, 15-22 https://doi.org/10.1002/9781119093220.ch2 https://doi.org/10.1007/978-3-319-48220-0_2

Pfennig A., Zastrow P., Kranzmann A. (2013). Influence of heat treatment on the corrosion behaviour of stainless steels during CO_2-sequestration into saline aquifer, International Journal of Green House Gas Control, 15, 213–224 https://doi.org/10.1016/j.ijggc.2013.02.016

Pfennig, A. Kranzmann A. (2011). Reliability of pipe steels with different amounts of C and Cr during onshore carbon dioxid injection. International Journal of Greenhouse Gas Control, 5, 757–769. https://doi.org/10.1016/j.ijggc.2011.03.006

Pfennig, A., Wiegand, R., Wolf, M., Bork, C.-P. (2013).Corrosion and corrosion fatigue of AISI 420C (X46Cr13) at 60 °C in CO2-saturated artificial geothermal brine, Corrosion Science 68 (2013) 134–143. https://doi.org/10.1016/j.corsci.2012.11.005

Pfennig, A., Wolthusen, H., Kranzmann, A. (2017). Unusual corrosion behavior of 1.4542 exposed a laboratory saline aquifer water CCS-environment. Energy Procedia, 114, 5229-5240. https://doi.org/10.1016/j.egypro.2017.03.1678 https://doi.org/10.1016/j.egypro.2017.03.1679

Pfennig, A., Wolthusen, H., Wolf, M., Kranzmann, A. (2014). Effect of heat treatment of injection pipe steels on the reliability of a saline aquifer water CCS-site in the Northern German Basin Energy Procedia, 63, 5762-5772.

Seiersten M. (2001), Material selection for separation, transportation and disposal of CO_2, Corrosion paper no. 01042.

Thomas D.C. (2005). Carbon Dioxide Capture for Storage in Deep Geologic Formations – Results from CO_2 Capture Project, Volume 1: Capture and Separation of Carbon Dioxide form Combustion Sources, CO_2 Capture Project, Elsevier Ltd UK, ISBN 0080445748.

Unigovski, Ya.B., Lothongkum, G., Gutman, E.M., Alush, D., Cohen, R. (2009).Low-cycle fatigue behaviour of 316L-type stainless steel in chloride solutions, Corrosion Science, 51, 3014-3120. https://doi.org/10.1016/j.corsci.2009.08.035

Van den Broek M., Hoefnagels R., Rubin E., Turkenburg W., Faaij A. (2010). Effects of technological learning on future cost and performance of power plants with CO_2 capture,

in Projects Costs of Generating Electricity. Progress in Energy and Combustion Science,177-187

Vignal V., Delrue O., Peultier J., Oltra R. (2007). Critical Factors in Localized Corrosion 5: A Symposium in Honour of Hugh Isaacs, Local mechanical-electrochemical behavior of duplex stainless steels. The Electrochemical Society, 102-104

Wei, L., Pang, X., Liu, C., Gao, K. (2015). Formation mechanism and protective property of corrosion product scale on X70 steel under supercritical CO_2 environment. Corrosion Science, 100, 404–420. https://doi.org/10.1016/j.corsci.2015.08.016

Wolf M., Afanasiev R., Böllinghaus T., Pfennig A. (2016). Investigation of Corrosion Fatigue of Duplex Steel X2CrNiMoN22 5 3 Exposed to a Geothermal Environment under Different Electrochemical Conditions and Load Types, 13th International Conference on Greenhouse Gas Control Technologies, GHGT-13, 14th -18th November 2016, Lausanne, Switzerland.

Wu S.L, Cui Z.D., Zhao G.X., Yan M.L., Zhu S.L., Yang X.J. (2004). EIS study of the surface film on the surface of carbon steel form supercritical carbon dioxide corrosion. Applied Surface Science, 228, 17-25. https://doi.org/10.1016/j.apsusc.2003.12.025

Zhang H., Zhao Y.L, Jiang Z.D. (2005). Effects of temperature on the corrosion behaviour of 13Cr martensitic stainless steel during exposure to CO_2 and Cl^- environment, Material Letters, 59, 3370-3374 https://doi.org/10.1016/j.matlet.2005.06.002

Zhang L., Yang J., Sun J.S., Lu M. (2008). Effect of pressure on wet H_2S/CO_2 corrosion of pipeline steel, No. 09565, NACE Corrosion 2008 Conference and Expo, New Orleans, Louisiana, USA, March 16th – 20th

Zhang L., Zhang W., Jiang Y., Deng B., Sun D., Li J. (2008). Influence of annealing treatment on the corrosion resistance of lean duplex stainless steel, NACE Corrosion 2008 Conference and Expo, New Orleans, Louisiana, USA, March 16th – 20th